

Phase Detrending for Measured Multisine Signals^{*}

Kate A. Remley,¹ Dylan F. Williams,¹ Dominique M. M-P. Schreurs,² Giovanni Loglio,³ and Alessandro Cidronali³

1. RF Technology Division, National Institute of Standards and Technology;
325 Broadway; Boulder, CO 80305 remley@boulder.nist.gov

2. K.-U.-Leuven; Div. ESAT-TELEMIC Kasteelpark Arenberg 10; B-3001 Leuven, Belgium

3. Dept. Electronics and Telecommunications; Univ. of Florence; Florence, 50139 Italy

Abstract: We develop a method to detrend the phases of measured multisine signals. We find a time reference that removes the linear component of the measured phases and aligns them, within a precision specified by the user, to their expected values. An initial guess is provided by a closed-form expression. We then find the global minimum of a user-specified error function. The simple post-processing algorithm is general and can be implemented in many software packages.

1. Introduction

Multisines consist of a collection of simultaneously generated sinewaves, typically with a constant frequency spacing Δf between them. They can be used in applications such as circuit and system characterization [1-3], model development and system identification [4-6], and to calibrate instrumentation such as nonlinear vector network analyzers [7, 8]. In some applications the relative phase relationships between the different frequency components are chosen randomly. There are also some types of multisines that have special phase relationships between the frequency components, including the constant-phase multisine and Newman and Schroeder multisines [4, 9]. The latter two have low peak-to-average power ratios and are sometimes used to approximate digitally modulated signals in design and test.

To physically generate a multisine signal, we specify the desired values of relative phase for each component on a signal source. The source will begin generating the multisine

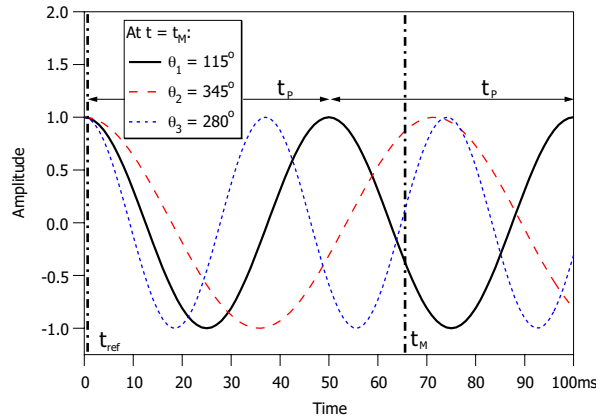


Figure 1: A multisine with three sinewave components having 0° relative phase at time t_{ref} . A measurement made at time t_M will yield relative phases having no obvious meaningful relationship. t_p is the repetition rate of the carrier (solid line). Note that while the phase of the carrier passes through 0° every t_p , it is only at t_{ref} that all frequency components line up with their specified values.

^{*} Work of the National Institute of Standards and Technology, not subject to U.S. copyright

at a certain point in time, which we will call the reference time t_{ref} . A subsequent measurement of the signal will be made by another instrument at some other time t_{M} during the repetitive signal generated by the source. The phases at t_{M} measured by the second instrument will not usually appear to correspond in any obvious way to those generated at t_{ref} due to the time difference $t_{\text{ref}} - t_{\text{M}}$, as illustrated in Fig. 1. If we can identify t_{ref} from a measurement made at t_{M} , we can shift our time reference back to t_{ref} and align the phases as they were when they were generated. Numerically determining t_{ref} from t_{M} is a central goal of this paper.

The methods of [10-12] were developed to find the relative phases of two-tone signals at the output of a nonlinear device. These methods are based on cancellation of a reference signal at the output of the device. The method of [13] was developed to find complex ratios of the frequency components of harmonically related signals, and can be used to determine the phases of the frequency components of multisine signals relative to a reference signal. This method requires the use of a reference signal to establish a time reference, and that reference must be at the fundamental frequency to establish unique phase relationships between the different frequency components of the multisines. The process of detrending described here does not require external measurement of a reference signal nor a reference signal at the fundamental.

The process of aligning measured phases has often been carried out in the frequency domain, and is called phase detrending. Phase detrending is accomplished by subtracting a linear phase from each frequency component of the multisine signal. The problem with this method is that the phase of each frequency component of the multisine repeats modulo 2π , complicating the process. However, subtracting a linear phase from a multisine signal, which corresponds to multiplication by $e^{-j2\pi f t}$ in the frequency domain, is equivalent to adding a delay to the signal in the time domain. So phase detrending also can be thought of in terms of a shift in time. This is the approach we take in this paper to phase detrending and alignment.

2. Phase Detrending and Alignment Procedure

For simplicity, we focus on finding the difference between t_{ref} and the arbitrary time t_{M} when a measurement of the phases of a multisine is made. That is, we find the quantity $t_{\text{ref}} - t_{\text{M}}$. The procedure has two parts. First we find a closed-form estimate for $t_{\text{ref}} - t_{\text{M}}$. Then we use a simplex search method [14] to iterate on an error function and identify a global minimum that best aligns the measured phases with their expected values to within a user-specified precision. We demonstrate that a change of variables can provide simple, integer starting points for the search method.

We define the envelope of the multisine signal from the sum of its sinewave components. The period T of the envelope corresponds to $1/\Delta f$, where Δf is the spacing between two adjacent tones. For a measurement made at t_{M} , we can estimate the value of t_{ref} in the interval $[0, T]$ if we have an expected value for at least two adjacent sinewave components. Using adjacent tones places the most stringent condition on alignment, as theoretically there will be only one time in the envelope where the phases of adjacent components simultaneously pass near their expected values.

We begin by expressing the phase $\theta_i(t)$ of the i^{th} component of the multisine at time t in terms of its measured value $\theta_i(t_M)$ at time t_M . $\theta_i(t)$ is related to $\theta_i(t_M)$ by

$$\theta_i(t) = \theta_i(t_M) + 2\pi f_i(t - t_M), \quad (1)$$

where f_i is the frequency of the i^{th} component of the multisine.

Our initial estimate of $t_{\text{ref}} - t_M$ is based on an analytic expression that estimates a time where the phases of two adjacent sinewave components are close to their expected values. It is given by

$$(t_{\text{ref}} - t_M)_{\text{est}} = \frac{[\theta_1(t_M) - \theta_{1,\text{target}}] - [\theta_0(t_M) - \theta_{0,\text{target}}]}{2\pi(f_0 - f_1)} = \frac{[\theta_1(t_M) - \theta_{1,\text{target}}] - [\theta_0(t_M) - \theta_{0,\text{target}}]}{2\pi \text{sgn}(f_0 - f_1)} T. \quad (2)$$

Here, subscripts 0 and 1 refer to two adjacent frequency components, $|f_0 - f_1| = \Delta f$, and $\text{sgn}(x) = +1$ if $x > 0$, and $\text{sgn}(x) = -1$ if $x < 0$. The angles $\theta_0(t_M)$ and $\theta_1(t_M)$ refer to the measured phases of the frequency components and the subscript “target” refers to the expected value of the phase. Note that an expression similar to (2) is given in the Appendix of [8].

The numerator of the fractional part of (2) corresponds to a phase difference between two frequency components $\Delta\theta$, which difference can take on values between 0 and 2π over the period of the envelope. Since the frequency components are adjacent, any given value of $\Delta\theta$ should occur only once during T . This equation simply relates a fraction of the envelope period $(t_{\text{ref}} - t_M)/T$ to the fraction of 2π where the desired $\Delta\theta$ will be reached. To find the value of t_{ref} that provides an optimal solution for all frequency components of the multisine simultaneously, refinement of (2) is necessary.

In the real world, our measured phase values rarely correspond exactly to their specified values, due to signal generation and measurement errors and distortion. We define an error function as the mean-squared difference between our expected and measured values of phase¹ as

$$E(t) = \sum_{i=1}^N |\theta_i(t) - \theta_{i,\text{target}}|^2, \quad (3)$$

where N is the total number of frequency components in the multisine.

To refine the estimate of (2), we perform a search for the global minimum of the error function. Figure 2 shows a segment of the error function for a Schroeder multisine with seven components. The top half of the figure shows that there are many local minima spaced approximately $1/f_0$ apart, where f_0 is the carrier frequency of the multisine. Even though there are many times within T that correspond to local minima for the error function, there is only

¹The algorithm accommodates other error functions. For example, the user could specify an error function that minimizes the difference between the expected and measured vectors or a weighted version of (3).

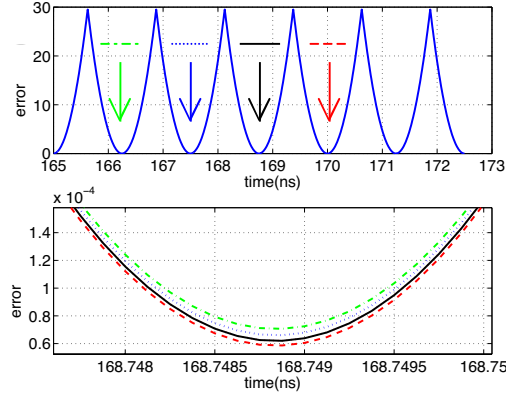


Figure 2: A time segment of the error function for a Schroeder multisine with seven frequency components. Top: Several local minima are evident with spacing of $\sim 1/f_0$ where f_0 is the frequency of the carrier. Bottom: Zoom-in of the top plot showing an overlay of four adjacent minima. The time labeled on the time axis corresponds to the solid curve, while the dashed and dotted curves correspond to adjacent and second-adjacent minima (shown in the top graph), time-shifted to illustrate the slight differences between them.

one global minimum. The bottom half of the figure shows only one absolute, or global, minimum.

We found that, based on the form of the error function shown in Fig. 2 above, we can greatly simplify the numerical solution process with a change to a new time-like variable k . This variable changes by one with each cycle of the carrier, which has frequency f_0 .² The new variable k is defined by³

$$k \equiv f_0 \cdot (t - t_M) - \frac{\theta_{0,\text{target}} - \theta_0(t_M)}{2\pi}. \quad (4)$$

The time t can be written in terms of k as

$$t(k) = \frac{2\pi k + \theta_{0,\text{target}} - \theta_0(t_M)}{2\pi f_0} + t_M, \quad (5)$$

and the expression for $\theta(t)$ in (1) can be rewritten as

$$\theta_i(k) = \theta_i(t_M) + f_i \left(\frac{2\pi k + \theta_{0,\text{target}} - \theta_0(t_M)}{f_0} \right). \quad (6)$$

² The frequency component f_0 is often, but need not always be, the carrier frequency. For example, in the case of two-tone excitation, f_0 is simply the frequency of one of the two tones.

³ In the implementation of the algorithm, we typically set $t_M = 0$ without loss of generality. This is a convenience that lets us focus on finding a real value for t_{ref} relative to the (usually) unknown time at which our measurements were made.

There are two advantages of this change of variables. First, whenever k is an integer, $\theta_0[t(k)] = \theta_{0,\text{target}}$. Thus, E is nearly zero, and the convergence to local minima E is extremely rapid if we begin our searches at integer values of k . Second, the search problem is nicely scaled if we search for local minima in E with respect to k , rather than the time t . This is because the local minima are roughly integer distances away in k , but roughly a distance of $1/f_0$, which is often small, in time.

We can rewrite the starting estimate in (2) as

$$k_{\text{est}} \approx \text{int} \left[\frac{f_0}{f_0 - f_1} \left(\frac{[\theta_1(t_M) - \theta_{1,\text{target}}] - [\theta_0(t_M) - \theta_{0,\text{target}}]}{2\pi} \right) - \frac{\theta_{0,\text{target}} - \theta_0(t_M)}{2\pi} \right], \quad (7)$$

where $\text{int}(x)$ is the integer part of x . Choosing the nearest integer k_{est} usually aligns the sinewave components to within a degree or so of the target phases for measurements without significant distortion. In some applications, the rough estimate of (7) is sufficiently accurate. Note that the second term on the righthand side of (7) is small and can usually be neglected, since our goal is simply to find a starting point for the search routine.

To find the global minimum, we begin searches for local minima at $k_{\text{est}} \pm n$ for $n = 0, 1, 2, \dots$ and select the lowest local minimum. We have found that starting our searches at integer values near k_{est} results in exceptionally quick and stable searches for local minima. Since the estimate of (7) [or, equivalently, (2)] puts us in the neighborhood of the global minimum, we usually do not need to search over more than ± 20 local minima to find the global minimum. To ensure that we have found the global minimum, we check to see that our lowest minimum is not at the edge of our search range. The result of this automated procedure is a refined estimate of the time reference t_{ref} and a set of phases at t_{ref} .

Once the global minimum t_{ref} is found that best detrends the measurements with respect to our minimized error function, (6) [or equivalently, (1)] can be used to determine the values of the phases θ_i at t_{ref} . We can also use (6) to determine the phases of other frequency components such as IM products for which there are no expected values, as discussed in the next section.

3. Comparing Measurements at the Input and Output of a Device

Figure 3 shows a typical measurement setup for a two-port amplifier. The signal source generates a multisine that is fed into the input of an amplifier or other device under test (DUT). The amplifier both delays and distorts the input signal as it amplifies it. Section 2 discussed how to go about detrending the phases of the signal at the input to the amplifier. Now, we will discuss finding a new reference time t_1 that detrends the signal at the amplifier's output, how to relate this time to the delay through the amplifier, and evaluating the amplifier's distortion.

After detrending the signal at the input of the amplifier, as before, the input signal is described by the reference time t_{ref} , as well as the amplitudes and phases of each frequency

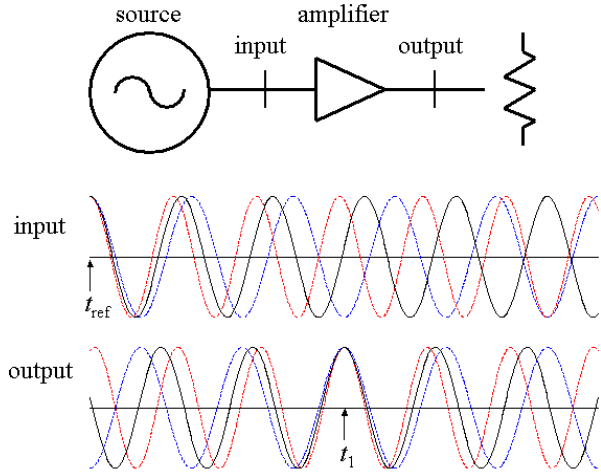


Figure 3: Top: Typical setup for measuring a multisine through an amplifier. Bottom: Phase relationships of the frequency components of the multisine at the input and output of the amplifier.

component of the multisine at t_{ref} . Along with this information on the signal at t_{ref} , we can use the same procedure to detrend the signal at the output of the amplifier. That is, we use measurements performed at time t_M and the preceding algorithms to estimate the time t_1 at which the signal arrived at the output.

Ideally, the signal at the output will look like an amplified copy of the signal at its input, so we set our target values for determining t_1 to the measured phases at t_{ref} at the amplifier's input. That is, we find an estimate for $t_1 - t_{ref}$ instead of $t_{ref} - t_M$. Using target values based on the phases at t_{ref} will provide us with the best estimate of the linear phase delay through the amplifier. Again we perform a minimization of the error function. Like the input signal, this output signal is now described by the reference time t_1 , and the amplitudes and phases of each frequency component of the multisine are found at t_1 .

We now have enough information to describe both the amplifier's linear phase delay (the propagation delay through the device plus any linear component of phase distortion) and higher-order phase distortion for this input signal. While sometimes difficult to measure accurately, the amplifier's linear phase delay is given by $t_1 - t_{ref}$, and its higher-order phase distortion is given by the difference of each frequency component's input phase at time t_{ref} and output phase at time t_1 .

4. Measurement Examples Using the Phase Detrending Algorithm

We present several examples illustrating the use of the phase detrending procedure in various applications. In all cases, a vector signal generator was used to produce the multisine signals, measurements were made using a nonlinear vector network analyzer (NVNA) [7], and the post-processing routine described above was used to detrend the phases. The carrier frequency f_0 was 800 MHz unless stated otherwise.

Example 1: Three-Tone, One-Port Example with Constant Relative Phases:

We generated a three-tone multisine signal with $f_L = f_0 - \Delta f$, f_0 , and $f_U = f_0 + \Delta f$. We considered three values of Δf : 25 kHz, 50 kHz, and 100 kHz. In this example, the phase of each tone was specified to be 0° .

We examined the phase of the excitation signal with port 2 of the NVNA open-circuited (a no-load case). Table 1 shows the measured phases, the phases based on the initial estimate of (7), and the detrended phases found by minimization of the global error function given in (3) for each Δf value. The final value of the minimized error function is also shown. Note that none of the detrended phases agree exactly with their targets: this is to be expected since neither the excitation nor the measurements are exact. However, the measured detrended phases are always within 0.3° of their target values.

| | $\Delta f = 25$ kHz (θ in degrees) | | | $\Delta f = 50$ kHz (θ in degrees) | | | $\Delta f = 100$ kHz (θ in degrees) | | |
|--------|---|-----------------------|-------------------------|---|-----------------------|-------------------------|--|-----------------------|-------------------------|
| | θ_{meas} | θ_{est} | θ_{final} | θ_{meas} | θ_{est} | θ_{final} | θ_{meas} | θ_{est} | θ_{final} |
| f_L | 10.75 | -0.0041 | 0 | -31.39 | 0.0073 | -0.028 | -88.26 | 0.0031 | 0.13 |
| f_0 | 16.59 | 0 | -0.14 | 47.21 | 0 | -0.26 | 137.69 | 0 | -0.28 |
| f_U | 22.85 | 0.43 | 0.12 | 126.59 | 0.77 | -0.29 | 4.48 | 0.82 | 0.15 |
| $E(t)$ | | 0.184 | 0.0345 | | 0.600 | 0.152 | | 0.686 | 0.115 |

Table 1: Measured and detrended phases of the three tones for three Δf values. The expected value of all three tones is 0° . θ_{meas} is the raw, measured data, θ_{est} has been aligned according to the initial estimate of (7), and θ_{final} is the detrended data based on minimization of (3). The final error-function values are shown in the last row.

Example 2: Three-Tone, One-Port Example with Differing Phases:

The second example we considered used the same three-component multisine and the same measurement setup, but 45° was added to the specified value of θ_L . We see in Table 2 that the final detrended value θ_L is always within 0.3° of 45° .

| | $\Delta f = 25$ kHz (θ in degrees) | | | $\Delta f = 50$ kHz (θ in degrees) | | | $\Delta f = 100$ kHz (θ in degrees) | | |
|--------|---|-----------------------|-------------------------|---|-----------------------|-------------------------|--|-----------------------|-------------------------|
| | θ_{meas} | θ_{est} | θ_{final} | θ_{meas} | θ_{est} | θ_{final} | θ_{meas} | θ_{est} | θ_{final} |
| f_L | -1.00 | 44.99 | 44.97 | 98.01 | 45.01 | 45.27 | -64.65 | 45.00 | 45.13 |
| f_0 | -58.79 | 0 | -0.13 | 76.47 | 0 | -0.28 | -174.42 | 0 | -0.32 |
| f_U | -71.19 | 0.40 | 0.15 | 100.76 | 0.82 | 0.0036 | 121.80 | 0.97 | 0.20 |
| $E(t)$ | | 0.158 | 0.0415 | | 0.676 | 0.152 | | 0.946 | 0.160 |

Table 2: Measured and detrended phases of the three tones for three different Δf values. The expected value of the relative phase of the lower tone was 45° , and the expected value of the other two was 0° .

Example 3: Seven-Tone, One-Port Schroeder Multisine:

The phases of the sinewave components of a Schroeder multisine can be specified analytically as [4]:

$$\phi_k = \frac{-k(k-1)\pi}{N},$$

where ϕ_k is the phase of the k^{th} sinewave component, and k goes from 1 to N total sinewave components.

We generated a seven-tone Schroeder multisine using the measurement setup described above. Again, we considered three Δf values: 25 kHz, 50 kHz, and 100 kHz. We measured the no-load case at Port 1. To find the initial estimate of t_{ref} given in (7), we used the phase of the carrier for θ_0 and the phase of the lower adjacent tone for θ_1 . The target and detrended measured phases are shown in Table 3. Here, we see agreement within 0.5° .

| target (radians) | target (degrees) | $\Delta f = 25$ kHz (degrees) | $\Delta f = 50$ kHz (degrees) | $\Delta f = 100$ kHz (degrees) |
|--------------------------|---------------------|----------------------------------|----------------------------------|-----------------------------------|
| 0 | 0 | 0.16 | 0.024 | 0.071 |
| $-2\pi/7$ | -51.43 | -51.35 | -51.50 | -51.41 |
| $-6\pi/7$ | -154.29 | -154.55 | -154.57 | -154.61 |
| $-12\pi/7$ ($2\pi/7$) | 51.43 | 51.89 | 51.84 | 51.68 |
| $-20\pi/7$ ($-6\pi/7$) | -154.29 | -154.32 | -154.18 | -154.18 |
| $-30\pi/7$ ($-2\pi/7$) | -51.43 | -52.47 | -51.39 | -51.32 |
| 0 | 0 | -0.36 | -0.22 | -0.22 |
| $E(t)$ | | 0.4481 | 0.3126 | 0.2502 |

Table 3: The target and measured phase values for a seven-tone Schroeder multisine excitation. Each row corresponds to the phase of one frequency component in the multisine. Measured results for three different Δf values are shown. The minimized error function (3) for the detrended phases is shown in the last row.

Example 4: An Amplifier with High and Low Distortion

We generated a seven-tone constant-magnitude and constant-phase multisine, with 0° relative phase between sinewave components, again using the same measurement setup. Our Δf was 50 kHz. Our DUT was an off-the-shelf, 20 MHz to 5 GHz, packaged amplifier having 9 dB of gain. As discussed in Section 3, we first detrended the phases at the input of the device and then used those values (the phases at time t_{ref} in Fig. 3) as the target phases for detrending at the output of the device (the phases at time t_1 in Fig. 3).

We show three results in Table 4. The first shows the one-port, no-load case, which corresponds to the excitation signal to be applied to the input of the device. The error function value of 1.66 corresponds to phase errors less than $\sim 1.2^\circ$ in each frequency component, as shown in the “Input” curve of Fig. 4(a).

| | $E(t)$ Input | $E(t)$ Output |
|-----------------|--------------|---------------|
| No-Load Case | 1.66 | --- |
| Low Distortion | 1.81 | 0.073 |
| High Distortion | 5.50 | 23.85 |

Table 4: The minimized error function of (3) for a seven-tone constant-magnitude and constant-phase multisine with $\Delta f = 50$ kHz. Results are shown for the excitation (the no-load case), and for both low and high distortion cases.

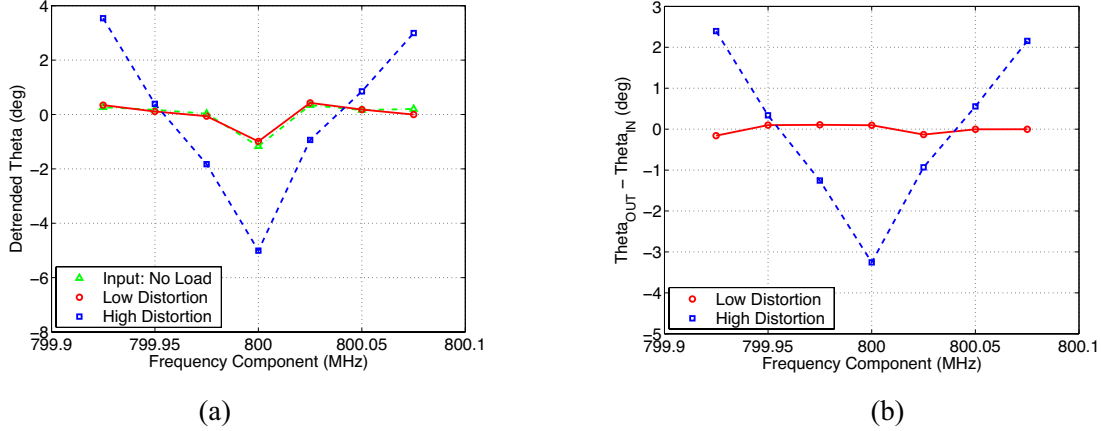


Figure 4: (a) The detrended, measured phases of the no-load excitation and the output signals. Note that when the amplifier is connected, the signal at the input port is nearly, but not exactly, equal to the no-load excitation. (b) Difference between the detrended, measured phases at the input port and the output port of the amplifier for low and high distortion.

In the Low Distortion result, the input signal level was low enough that the amplifier was operating in its “linear” region, and we expect little phase distortion. The complex input impedance of the amplifier causes an increase in the error function value at the input: from 1.66 for the no-load case to 1.81. There are also minor differences between the Input and Low Distortion curves in Fig. 4(a). As expected, the phases at the output are very similar to the input for this low-distortion case, with an error function of only 0.073. This is illustrated in Fig. 4(b).

In the High Distortion result, the input signal level was increased and the amplifier was driven well into its nonlinear region. Here we see significant higher-order phase distortion shown by both an increase in the input error function value from 1.81 to 5.50 and in the high output error function value of 23.85. Fig. 4(b) shows the corresponding differences between input and output phase values, clearly illustrating the increase in distortion at the higher input signal level.

Example 5: Two-Tone Signal Sweeps

We performed NVNA measurements of the same amplifier by sweeping the input voltage level from nominally 0.5 V to 1.0 V per tone, and sweeping Δf of the input tones from 1 kHz to 500 kHz. We specified 0° relative phase for both input tones. We measured

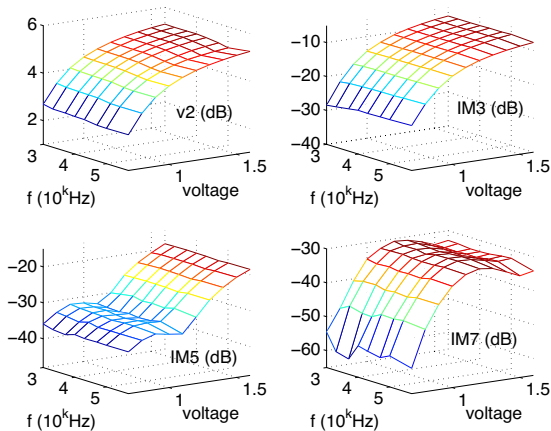


Figure 5: Magnitude (in dBV) of the output voltage v_2 at the upper fundamental, IM3, IM5, and IM7 frequencies.

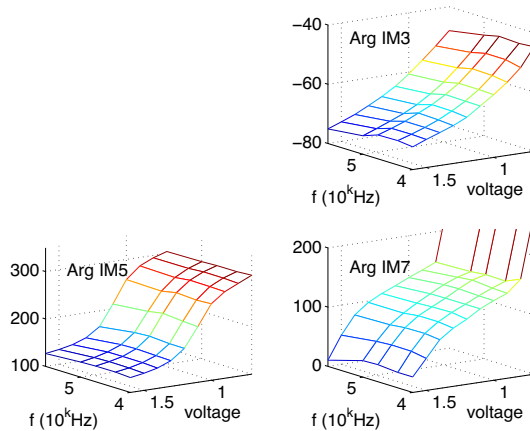


Figure 6: Phase (in degrees) of the output voltage v_2 at the upper IM3, IM5, and IM7 frequencies. The intermodulation products are referenced to the phase of the fundamental, so the phase of the fundamental is not shown. Note: the axes of these plots are rotated compared to those in Fig. 5 in order to resolve the phase values.

the output voltages at the excitation frequencies and the intermodulation products IM3 ($f_c \pm 3\Delta f$), IM5 ($f_c \pm 5\Delta f$), and IM7 ($f_c \pm 7\Delta f$). Results for the upper set of output tones at the excitation frequencies, IM3, IM5, and IM7 are shown in Figs. 5 and 6. Similar results were found for the lower set of tones.

Magnitude plots where the input-tone spacing and voltage levels are swept, such as those shown in Fig. 5, have been used for years to describe the nonlinear effects and frequency asymmetry of amplifiers [15]. Figure 6 shows the less-common swept-tone phase plot. These types of plots are used to characterize the slow memory effects of amplifiers as described in, for example, [16]. Use of the NVNA has greatly simplified these measurements compared to the procedures described in [10-12].

Here, as in Example 4, we see the effect of phase distortion at higher input voltage levels, shown in Fig. 6 by the change in the phase of the intermodulation products. Separating the linear phase delay (delay through the device plus any linear phase distortion) from other types of phase distortion is difficult in the two-tone case, since there will always be a point in the envelope of a two-tone signal where the phases of the two tones are aligned to a target value.

5. Conclusion

We have developed a procedure for detrending the phases of measured multisine signals using a straightforward post-processing scheme. The procedure is based on two simple steps: first we find a closed-form estimate of the delay between the time where a pair of measured phases pass through their specified values and the time our measurement was taken. Second, we refine that estimate by minimizing an error function that takes into account

all frequency components for which we have expected phase values. We extended this method to provide estimates of both the linear and higher-order distortion through a nonlinear device such as an amplifier. We demonstrated the effectiveness of the algorithm in several examples.

The algorithm developed here is easy to implement and execute, and we hope that it will provide a link between making multisine measurements and readily using them for system characterization and model development. Note that this procedure makes no reference to the carrier frequencies at the input and output of the DUT. Thus, this procedure will be equally applicable to mixers and other frequency converters where we expect the signal at the output to look like a delayed and distorted version of the input signal. Also, the phases of the harmonics of multisines may be detrended in a straightforward way, using the same time reference we found from the fundamental.

References:

- [1] J. C. Pedro and N. Borges de Carvalho, "On the use of multitone techniques for assessing RF components' intermodulation distortion," *IEEE Trans. Microwave Theory Tech.*, vol. 47, pp. 2393-2402, Dec. 1999.
- [2] R. Hajji, F. Beaugerard, and F. M. Ghannouchi, "Multitone power and intermodulation load-pull characterization of microwave transistors suitable for linear SSPA's design," *IEEE Trans. Microwave Theory Tech.*, vol. 45, pp. 1093-1099, July 1997.
- [3] J. Verspecht, F. Verbeyst, and M. Vanden Bossche, "Network analysis beyond S-parameters: characterizing and modeling component behaviour under modulated large-signal conditions," *56th ARFTG Conf. Dig.*, pp. 9-12, Dec. 2000.
- [4] R. Pintelon and J. Schoukens, *System Identification: A Frequency Domain Approach*. New York, NY: IEEE Press, 2001.
- [5] W. van Moer, Y. Rolain, and A. Geens, "Measurement based nonlinear modeling of spectral regrowth," *IEEE MTT-S Int. Microwave Symp. Dig.*, pp. 1467-1470, 2000.
- [6] G. Simon and J. Schoukens, "Robust broadband periodic excitation design," *IEEE Trans. Instrum. and Measurement*, vol. 49, pp. 270-274, Apr. 2000.
- [7] T. Van den Broeck and J. Verspecht, "Calibrated vectorial nonlinear-network analyzers," *IEEE MTT-S Int. Microwave Symp. Dig.*, pp. 1069-1072, 1994.
- [8] A. Barel and Y. Rolain, "A microwave multisine with known phase for the calibration of narrowbanded nonlinear vectorial network analyzer measurements," *IEEE MTT-S Int. Microwave Symp. Dig.*, pp. 1499-1502, 1998.
- [9] S. Boyd, "Multitone signals with low crest factor," *IEEE Trans. Circuits Syst.*, vol. CAS-33, pp. 1018-1127, Oct. 1986.
- [10] N. Suematsu, Y. Iyama, and O. Ishida, "Transfer characteristic of IM3 relative phase for a GaAs FET amplifier," *IEEE Trans. Microwave Theory Tech.*, vol. 45, pp. 2509-2514, Dec. 1997.
- [11] Y. Yang, J. Yi, J. Nam, B. Kim, and M. Park, "Measurement of two-tone transfer characteristics of high-power amplifiers," *IEEE Trans. Microwave Theory Tech.*, vol. 49, pp. 568-571, Mar. 2001.
- [12] B. Kim, Y. Yang, J. Cha, Y. Y. Woo, and J. Yi, "Measurement of memory effect of high-power Si LDMOSFET amplifier using two-tone phase evaluation," *60th ARFTG Conf. Digest*, Dec. 2002.
- [13] J. A. Jargon, D. C. DeGroot, K. C. Gupta, and A. Cidronali, "Calculating ratios of harmonically related, complex signals with application to nonlinear large-signal scattering parameters," *60th ARFTG Conf. Dig.*, pp. 113-122, 2002.
- [14] J. C. Lagarias, J. A. Reeds, M. H. Wright, and P. E. Wright, "Convergence properties of the Nelder-Mead simplex method in low dimensions," *SIAM J. Optimization*, vol. 9, pp. 112-147, 1998.
- [15] S. C. Cripps, *RF Power Amplifiers*. Boston: Artech House, 1999.
- [16] H. Ku, M. D. McKinley, and J. S. Kenney, "Quantifying memory effects in RF power amplifiers," *IEEE Trans. Microwave Theory Tech.*, vol. 50, pp. 2843-2849, Dec. 2002.